Journal of the Australian Ceramic Society (2022) 58:1231–1240
https://doi.org/10.1007/s41779-022-00739-w

RESEARCH

Preparation and characterization of pure natural hydroxyapatite derived from seashells for controlled drug delivery

Serap Ayaz Seyhan[1,2] · Dilek Bilgic Alkaya[1,2] · Sumeyye Cesur[1] · Faik Nuzhet Oktar[1,3] · Oguzhan Gunduz[1,4]

Received: 25 November 2021 / Revised: 30 March 2022 / Accepted: 1 April 2022 / Published online: 24 May 2022

Abstract

The marine species are specially used for the fabrication of bioceramic nano-powders with natural methods for their use in controlled drug delivery. However, there are only very limited studies regarding the production and synthesis of hydroxyapatite (HA)–based drug delivery systems from marine structures. In this study, poly (vinyl alcohol) (PVA) containing Rifampicin (RIF)–loaded Orange Spiny Oyster Seashell (*Spondylus barbatus*) hydroxyapatite (HA) composite is synthesized by an in situ ultrasound-assisted method. All samples were analyzed by X-ray diffraction (XRD), Fourier transforms infrared (FTIR) spectroscopy, and Scanning electron microscope (SEM), respectively. The in vitro drug release tests of the obtained samples were performed in a phosphate-buffered medium (PBS) at 37 °C. Drug release was evaluated according to five varying kinetic models. In vitro RIF release from HA/PVA composite in phosphate buffer (pH 7.4) showed prolonged sustained drug release. From the drug release kinetic models, Higuchi and Korsmeyer–Peppas were found to be the best model for the three ratios based on the correlation coefficient. The diffusion component is less than 0.5, which indicates quasi-fickian diffusion. From the kinetic study results, the RIF-loaded marine phase composite has potential use in drug delivery applications as it shows positive sustained drug release behavior.

Keywords Hydroxyapatite · Poly (vinyl alcohol) · Rifampicin · Polycomposite · Drug delivery · Kinetic model

Introduction

Orange Spiny Oyster (Fig. 1) which is also called a bearded thorny oyster, lives along the Indo-West Pacific: from Indonesia to the Philippines; north to Japan, and south to (Australia). A seashell contains approximately 98% calcium carbonate. Lertcumfu et al. reported that hydroxyapatite (HA) prepared from marine materials as a raw material has excellent biocompatibility and bioactivity in vitro [1]. HA has a wide variety of applications in orthopedics and dentistry, because of its similarity to the components of human bone and teeth structures [2]. HA can be processed by a variety of chemical techniques (i.e., wet chemical, hydrothermal, solid-state reaction, sol–gel, and microwave methods) [3]. It has been confirmed that hotplate stirring is the most straightforward procedure for the production of HA from calcite/aragonite powders [4]. HA is also produced from bone or tooth dentin and enamel via the calcination method [3]. Many seashell combinations have been studied for the production of calcium phosphate materials. Also, there are many studies on marine-originated materials, which prove their osteoinductive properties and their biocompatibility [4]. Biological apatite such as seashells [1, 4], animal bone [5], and land snails [6], attract special attention due to the substitutions at the OH, Ca^{2+}, and PO_4^{3-} sites of HA, and the presence of several trace elements can enhance the overall biological performance of the biomaterial [7]. These trace elements play a crucial role in the performance of hard tissue. Also, it has been claimed that biological HA, due to its similarity to bone apatite, leads to comparable or even better overall properties and behavior than synthetic ones. Thus, efficient and low-cost methods to obtain HA from natural sources are gaining interest in the last years [8].

✉ Serap Ayaz Seyhan
sayaz@marmara.edu.tr; serapayz@gmail.com

1 Center for Nanotechnology & Biomaterials Application and Research (NBUAM), Marmara University, Istanbul, Turkey

2 Department of Analytical Chemistry, Faculty of Pharmacy, Marmara University, Istanbul, Turkey

3 Department of Bioengineering, Faculty of Engineering, Marmara University, Istanbul, Turkey

4 Department of Metallurgy and Materials Engineering, Faculty of Technology, Marmara University, Istanbul, Turkey

Fig. 1 Image of Orange Spiny Oyster Seashell (*Spondylus barbatus*)

Recently, HA [$Ca_{10}(PO_4)_6(OH)_2$] demonstrated essential for clinical applications and biomedical fields due to its extraordinary features [3, 6, 9]. Thus, HA composites or particles, including HA, have been selected recently in controlled drug delivery studies [10]. In recent years, the studies purposing to use ceramic/polymer materials as drug carriers, have also gained prominence [11–13]. Poly (vinyl alcohol) (PVA), which is a polymeric biomaterial, has achieved popularity due to intrinsic non-toxic, good biocompatibility, non-carcinogenicity, and desired physical properties [14]. It is widely used in the treatment of defects in load-bearing joint applications, drug delivery, and a scaffold supporting material for tissue engineering [13]. PVA is water-soluble and a low-cost and biocompatible polymer [15, 16]. In the literature, studies on the use of HA-reinforced PVA nanocomposites have been lately reported [17]. In this regard, a biocomposite material composed of HA and PVA can enhance as carriers for drug delivery owing to their unique biocompatibility, low production cost, low toxicity, easily tunable physical–chemical properties, and others [18].

The drug release mechanism depends on many factors. Therefore, it is significant to designate a release mechanism before applying. Mathematical models are also used for determining release kinetics. Besides, these models can contribute optimization of the release process [19, 20]. Rifampicin (RIF) [molecular weight: 822.94 g/mol, absorption max (pH 7.38): 237, 255, 334, 475 nm, soluble in methanol, slightly soluble in water] is a commonly used classic antibiotic against *Mycobacterium tuberculosis* and leprosy [21].

In this study, the oyster shell was synthesized by an in-situ ultrasound-assisted and hot-plate method. For comparison, HA nanocomposites were prepared both in the presence of PVA and in the absence of PVA. In addition, the interaction between RIF and different nanocomposites (HA and HA/PVA) was investigated. Then, the release of RIF from the two types of nanocomposite supports was studied and discussed. To predict and correlate the in vitro drug release behavior from formulated various RIF-loaded nanocomposites, it is necessary to fit into a suitable mathematical model. Drug release profiles were evaluated according to five different kinetic models (Korsmeyer-Peppas, Hixson-Crowell, zero order, first order, and Higuchi). It is very important to know how to use these equations to understand the different factors that affect the release velocity and how the dissolution behaviors can vary and influence the efficiency or the therapeutic regimen of patients. The concept, definitions, and physicochemical properties involved in each model are discussed and the equations are reported. The major aims of this research are twofold: (i) optimization of and biocompatible of a PVA nanocomposite reinforced by HA derived from Orange Spiny Oyster Seashell (Fig. 1) as an effective carrier of the drug therapy in future studies; and (ii) the development of an in vitro kinetic model for drug release about the synthesis method and PVA effect.

Materials and methods

Materials

PVA (Mw = 89,000–98,000, 99% hydrolyzed), and RIF were purchased from Sigma Aldrich USA. Orthophosphoric acid, PBS (phosphate buffer solution) (pH 7.4: 0.1 M) was purchased from Merck. Orange Spiny Oyster Seashells were collected from a local shop in Istanbul, Turkey. All other chemicals and solvents were of analytical grade. Double distilled water was used for rinsing and preparing solutions in the study.

Preparation of nanocomposites

Preparation of HA from Orange Spiny Oyster Seashell

First, the empty seashells were washed several times under tap water and dried to get rid of all possible rock, sand, and mussel fragments. It was then milled into fine particles in a porcelain mortar. The milled powder was sifted using a 100 µm sieve. The same production method used in our previous studies was carried out [4, 9]. 1 g of powder was

suspended in a certain volume of a water-filled beaker [3]. The solutions were placed on an ultrasonic bath at 80 °C for 15 min and, then according to the results of thermal analysis, the required volume of H_3PO_4 was calculated to set the stoichiometric molar ratio of Ca/P = 1.67 of HA, and later H_3PO_4 was added to the solution. To complete the reaction, the system was placed in an ultrasonic bath at 80 °C for 2 h. Afterward, the same procedure was carried out for the hot-plate method. The obtained solution was kept overnight at 25 °C, then centrifuged; a washing step was carried out with distilled water (several times to remove organic matter) and dried in a vacuum oven at 100 °C for 24 h to evaporate the liquid part and the resultant dried sediments were collected [5].

Preparation of HA/PVA, HA/RIF and HA/PVA/RIF nanocomposites

The synthesis of HA nanocomposites was performed in situ in the presence of PVA, and for comparison, pure HA was produced in the absence of PVA with the same method. The preparation of HA nanocomposites in the presence of polymer was followed as 1 g of crude powder was slowly added to the polymer (1% PVA; 250 mg /25 mL) solution; in the preparation of HA/RIF nanocomposite: 1 g of the raw powder was slowly added to RIF (25 mg/25 ml) solution; in the preparation of HA/PVA/RIF nanocomposite: 1 g of the raw powder was slowly added to polymer (1% PVA; 250 mg/25 mL) and RIF (25 mg/25 mL) solution and all samples were stirred in an ultrasonic bath at 80° C for 15 min. The equivalent amount of H_3PO_4 solution was added drop by drop into all solutions. The obtained solutions with and without biopolymer were kept overnight at 25 °C, then centrifuged, washed with distilled water, and dried in a vacuum furnace at 100 °C for 24 h [5].

Characterization of nanocomposites

XRD analysis was carried out by Bruker AXS D8 Advance system (Bruker, USA), equipped with a copper radiation source (Cu Kα, λ = 1.5418 Å) in the step-scanning mode. The XRD patterns were recorded in the 2θ range of 10–80°, with a step size of 0.02 and step duration of 0.5 s. Chemical interaction was investigated using a Fourier-transformed infrared (FT-IR) spectrometer (Jasco FT / IR-4700). The measurements were taken at an average resolution of 4 cm^{-1} and 4000–450 cm. The morphology of the biocomposite material before and after drug release was examined by scanning electron microscopy (SEM) (EVA MA 10, ZEISS, USA). The determination of the exact $CaCO_3$ content was made using DSC-DTA-TG equipment (TA SDTQ600 Protherm).

In vitro drug release experiments

Release of RIF from nanocomposites

To study the drug release kinetics, RIF-loaded nanocomposites (HA/RIF, HA/PVA/RIF) were weighed at 10 mg each (containing 0.25 mg RIF) and then, immersed in a 2 mL of PBS (pH 7.4 at 37 °C) with a constant stirring rate (200 rpm) for a period of 8 h in the orbital shaker-incubator (BIOSAN ES-20). At the defined time intervals (15, 30, 45, 60, 90, 120, 180, 240, 300, 360, 420, and 480 min) PBS was removed from each sample, and 2 mL of PBS was added again to continue the release test. UV spectroscopy (Shimadzu UV-1601) was used for monitoring the RIF releasing profile at 335 nm and 475 nm. The accumulated release of RIF was evaluated using the calibration graph of a standard RIF. The concentration ranges of RIF were 0.025–0.400 µg/mL. The calibration equation for RIF is $y = 0.3032x + 0.003$; $r^2 = 0.9999$ (for 335 nm), $y = 0.1744x + 0.0008$; $r^2 = 0.9999$ (for 475 nm) (Supplementary information, Fig. S1, S2). Each test was repeated three times during the study.

Adsorption of RIF onto HA/PVA nanocomposite

100 mg HA/PVA nanocomposite powder was added to 5 mL RIF solution (5 mg/5 mL). The solution was stirred at 200 rpm/min in the orbital shaker incubator (BIOSAN ES-20) at ambient temperature (25 °C) for 24 h. Afterward, the sample was removed from the solutions. To study the drug release kinetics, measurements were performed using the same procedure as explained above.

All measurements were repeated three times. The mass change (M) was calculated according to the following formula:

$$M(\%) = \frac{Mt - M0}{M0} x100$$

where M_0 and M_t are the mass of the sample before and after immersion in PBS, respectively.

Results and discussion

Characterization of nanocomposites

Figure 2 has shown the DSC-DTA-TG results of the raw powders. The decomposition of $CaCO_3$ to CaO was obtained in the curve. This curve approves that the shell consists of CaCO3. Thus, the calculation of the amount of H_3PO_3 solution is required to satisfy the demanded Ca/P ratios as possible. In Fig. 3 (bottom), the XRD pattern of

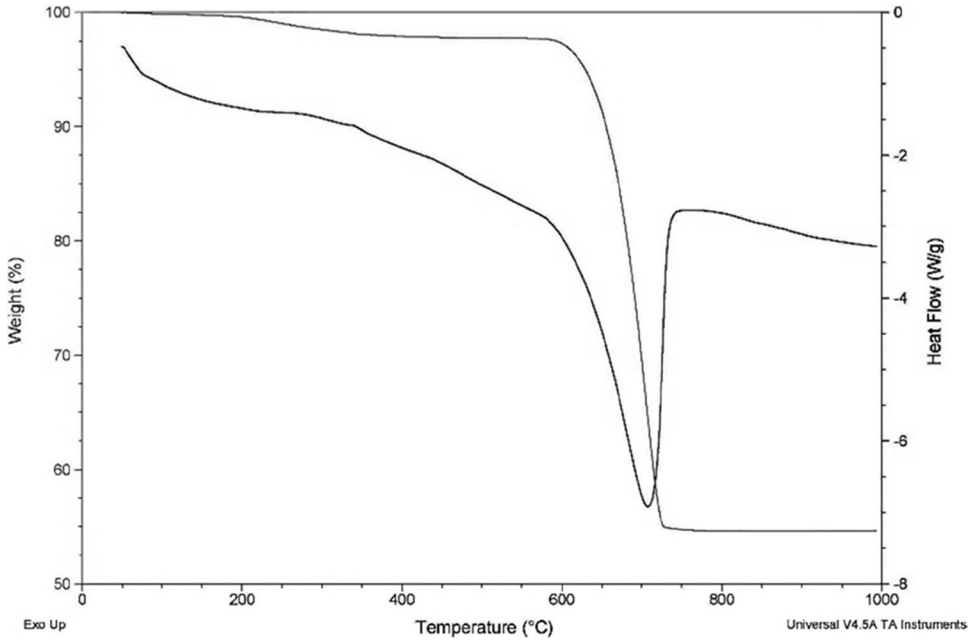

Fig. 2 DSC-DTA-TG analysis for the seashell sample

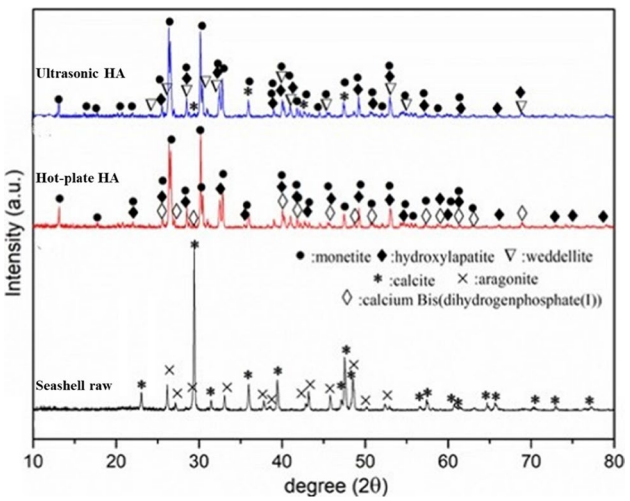

Fig. 3 X-ray diffractograms of HA samples

raw seashell powders is indicated. On the pattern, the main phase is a calcium carbonate that is aragonite (JCPDS card no: 00–076-0606) and calcite (JCPDS card no: 00–005-0586) [22]. It is seen that most of the aragonite structure had changed to HA or monetite ($CaHPO_4$) [23]. The XRD patterns of the samples which were produced from seashells are demonstrated in Fig. 3. In addition, XRD patterns of the samples produced by hot plate and ultrasonic method are included in Fig. 3. Figure 3 (mid) contains most of the hydroxyapatite peaks (JCPDS card number: 98–005-2689). Additionally, it is also detected that there are other phases such as monetite (JCPDS card no: 98–000-5429) [7]. It is already known that monetite also quickly transforms to TCP (tricalcium phosphate) structures. Monetite is used in the powder components of self-hardening calcium phosphate (CaP) pastes, which are used for skeletal repair [10]. Figure 3 (upper) contains most of the hydroxyapatite peaks (JCPDS card number: 98–005-2689) and it is also detected that there are other phases such as monetite (JCPDS card no: 98–000-5429), calcite (JCPDS card no: 00–041-1475) [24]. The results of FTIR analysis of the molecular structure for the HA and HA/PVA powders were indicated in Fig. 4. The OH modes (3569 cm^{-1} and 632 cm^{-1}), the P-O stretching modes (1091, 1044–1032 and 962 cm^{-1}), the O–P–O bending modes (602, 575–561 cm^{-1}), and the O-PO stretching modes (473, 463–460 cm^{-1}) from the PO_3–4 groups which are characteristic peaks of hydroxyapatite, are identified in all of the samples [25]. Since the samples were not sintered before FTIR analysis, the OH stretching mode at 3569 cm^{-1} was partially hidden by the water band between 2500 and 3800 cm^{-1}. These spectra are in agreement with the obtained XRD results. Figure 4(e) shows characteristic infrared bands of PVA polymer. The comparison of the FT-IR spectrum for the HA particles synthesized in the presence of polymer (Fig. 4(g)) with the spectra shown in Fig. 4(d) and (e) shows that there is a decrease in the intensity of the absorption bands associated with the OH suggesting the contribution from the similar groups in the PVA polymer [17]. Figure 4(f) shows characteristic peaks of RIF, at 3305 (-OH stretching), 2917 (-CH_3 stretching), 1735 (C = O carbonyl stretching), 1250 (C–O–C), and 895 cm^{-1} [26]. The FT-IR spectrum of HA/PVA/RIF (Fig. 4(f)) and the spectrum of HA/PVA shown in Fig. 4(g) were compared, it was seen that the characteristic RIF peaks disappeared. This could be due to the overlapping of the drug by the presence of excess carriers.

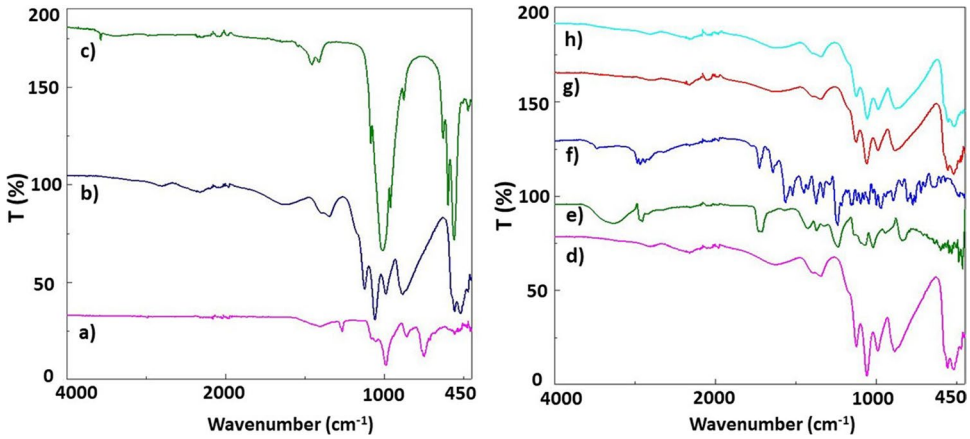

Fig. 4 Comparison of FTIR spectra of **a**) oyster seashell, **b**) HA synthesized from orange oyster shell, **c**) commercial HA, **d**) HA synthesized from orange oyster shell, **e**) pure PVA, **f**) RIF, **g**) HA/PVA, **h**) HA/PVA/RIF

Figure 5 and Fig. 6 represent the SEM micrographs of HA nanocomposites prepared in the presence and absence of PVA. Overall morphology for HA nanocomposites shows the regular distribution of spherical and rice-formed nanoparticles [5]. HA-PVA nanocomposite reveals a porous microstructure with mineral and polymer phases thus forming a highly homogeneous nanocomposite (Fig. 6(a,b)). It is observed that RIF, showing a rod-like structure due to its superior crystallinity, accumulated on the surface and pores of the drug-loaded samples (Fig. 5(c,d), Fig. 6(c,d,e,f) [26]. Whereas in nanocomposite of HA/RIF and HA/PVA/RIF (in situ), RIF rods are embedded in the nanocomposite matrix forming a compact block (Fig. 5(c,d) and Fig. 6(c,d)). However, in the HA/PVA/RIF (onto) nanocomposite, the porous HA/PVA layer is coated with the drug (Fig. 6(e, f)). It was observed that in situ synthesis did not affect the formation of particle sizes considerably.

In vitro drug release assay

To examine the applicability of HA nanocomposites as drug carriers, in vitro release behavior in a PBS (pH 7.4) solution medium was studied at 37 °C. (Fig. 7a spectrum).

All the nanocomposites displayed a similar drug release pattern with an initial release followed by a reduced release rate, as often described in the literature [27–30]. According to the results obtained, the release rate of RIF was fast in the first hour, and then it was observed, that it slowed

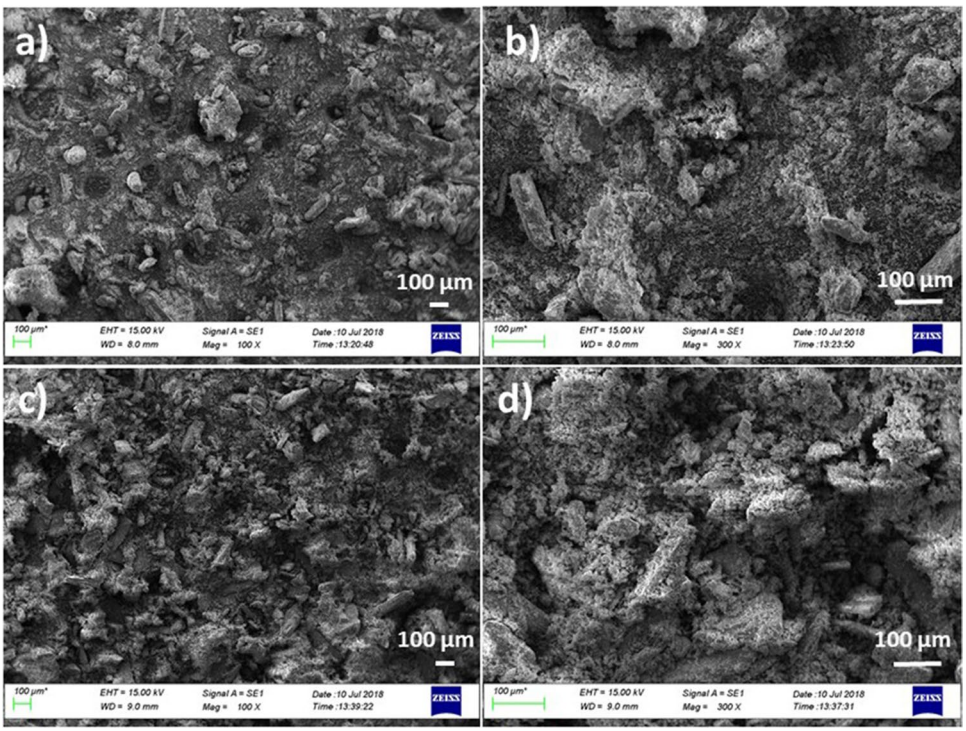

Fig. 5 SEM images of nanocomposite samples at high and low magnification; (**a**, **b**) HA, (**c**, **d**) HA/RIF

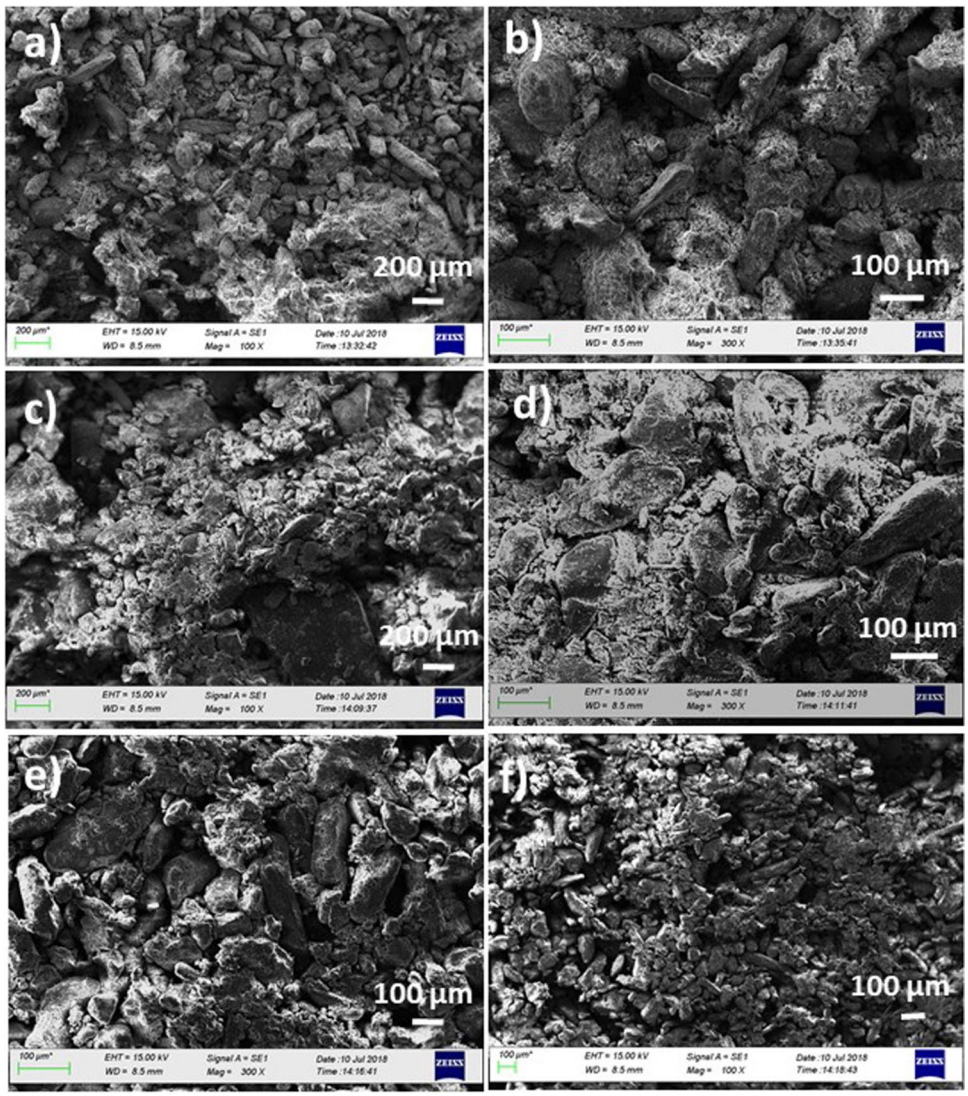

Fig. 6 SEM images of nanocomposite samples at high and low magnification; (**a**, **b**) HA/PVA, (**c**, **d**) HA/PVA/RIF, (**e**, **f**) HA/PVA/RIF loaded

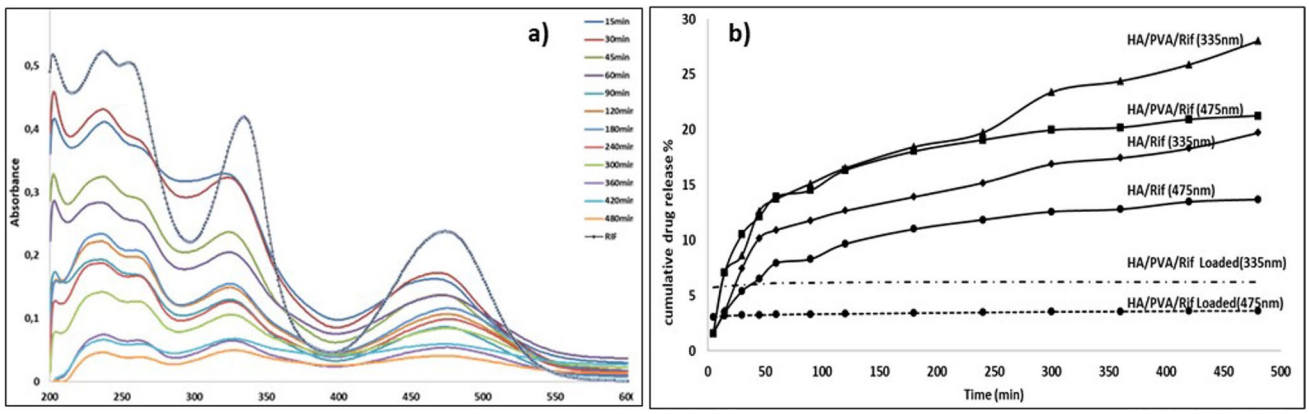

Fig. 7 **a** RIF spectrum of the nanocomposite samples in PBS solution and the spectra of the release of RIF from the nanocomposite. (**b**) Drug-release profiles for nanocomposites prepared with different variables (and different wavelengths: 335–475 nm)

Table 1 The correlation coefficient of the linear regressions of fitting release profiles by different kinetic models and release exponents for nanocomposites

Sample (335 nm)	Zero order		First order		Higuchi		Korsmeyer-Peppas			Hixson-Crowell	
HA/Rif	r^2	K_o	r^2	K_1	r^2	K_H	r^2	n	K_{KP}	r^2	K_{HC}
	0.8084	0.0304	0.8315	0.00046	*0.9275*	0.8133	0.9096	0.4929	1.0912	0.8239	0.0005
HA/PVA/Rif	r^2	K_o	r^2	K_1	r^2	K_H	r^2	n	K_{KP}	r^2	K_{HC}
	0.7105	0.0306	0.7381	0.00046	*0.8676*	0.8438	0.8250	0.4588	1.5962	0.7291	0.0005
HA/PVA/Rif load	r^2	K_o	r^2	K_1	r^2	K_H	r^2	n	K_{KP}	r^2	K_{HC}
	0.5355	0.0007	0.5360	0.00007	0.7287	0.0215	*0.9233*	0.0189	5.6092	0.5358	0.00005
Sample (475 nm)	Zero order		First order		Higuchi		Korsmeyer-Peppas			Hixson-Crowell	
HA/Rif	r^2	K_o	r^2	K_1	r^2	K_H	r^2	n	K_{KP}	r^2	K_{HC}
	0.8745	0.0448	0.9026	0.00046	*0.9631*	1.1737	0.8969	0.5201	1.2791	0.8937	0.0008
HA/PVA/Rif	r^2	K_o	r^2	K_1	r^2	K_H	r^2	n	K_{KP}	r^2	K_{HC}
	0.8086	0.0217	0.8218	0.00023	*0.9877*	0.5838	0.9499	0.4396	1.0638	0.8175	0.0004
HA/PVA/Rif load	r^2	K_o	r^2	K_1	r^2	K_H	r^2	n	K_{KP}	r^2	K_{HC}
	0.9160	0.0011	0.9165	0.00001	0.9391	0.0279	*0.9635*	0.0386	2.8248	0.9163	0.00002

K_0 is the release kinetic constant

K_1 is the release kinetic constant

K_H is the Higuchi's release kinetic constant

K_{KP} is the Korsmeyer-Peppas's release kinetic constant and n is the release exponent

K_{HC} is the Hixon-Crowelli's release kinetic constant

down relatively. After 8 h, the cumulative release rate of RIF reaches 19%, 28%, 6% and 13%, 21%, 4%, respectively HA/RIF, HA/PVA/RIF, and HA/PVA/RIF loaded (335 nm, 475 nm) in PBS (Fig. 7b cumulative%). Furthermore, RIF is not completely released, and the release curves reach plateaus after 8 h [31]. The examination of data (Fig. 7b) revealed that the release rate of RIF from adsorbed on the HA/PVA composite surface samples (HA/PVA/Rif Loaded) was very fast. Because PVA is an almost linear polymer, the interaction between the drug and the outer surface of the porous HA in the produced HA/PVA nanocomposite is weakened due to the polymer [29].

The results show that the release rate of RIF from HA (HA/Rif) is slower than the release from HA/PVA (HA/PVA/Rif with in situ synthesis) [31]. This has been interpreted as the fact that HA in the polymer structure accelerates the polymer degradation by increasing the porosity and facilitating the entry of water into the microspheres depending on its polar structure, thus accelerating the drug release [30]. It was concluded that the HA/PVA nanocomposite would be advantageous as a carrier medium for the hydrophobic drug RIF (Therapeutic dosage for RIF suggested is 15 mg/kg bodyweight (max. 900 mg) 2 or 3 times weekly or 10 mg/kg body weight single daily dose (max. 600 mg) in combination with other anti-mycobacterial agents), since the immediate release-limiting feature of HA would help prevent overdose [32].

In vitro drug release kinetics

The drug release kinetics and mechanism were appreciated mathematically according to five different kinetic models Zero Order, First Order, Higuchi, Hixson-Crowell, and Korsmeyer-Peppas model [33]. The release kinetics and parameters of each model were achieved by linear regression analysis (Supplementary information, Fig. S3–S32). The regression coefficients (r^2) were used to confirm the accuracy of the fittings (Table 1). Considering the regression results, three kinetic models (zero, first, and Hixson-Crowell) are not appropriate models to fit release. However, for both wavelengths and production techniques, drug release from HA, and HA/PVA nanocomposite samples can be fitted by the Higuchi model, and HA/PVA/RIF-loaded samples can be fitted by the Korsmeyer-Peppas model [34]. Again, the Higuchi and Korsmeyer–Peppas model was employed in the in vitro drug release behavior analysis of these formulations to distinguish between competing release mechanisms: Fickian release (diffusion-controlled release), non-Fickian release (anomalous transport), and case-II transport (relaxation-controlled release). When the n value is ≤ 0.43, it is the Fickian release. When n values are observed between 0.43 and 0.85, diffusional mass transport and polymer chain relaxation may both be rate-controlling processes. In such cases, transport is commonly called non-Fickian release (anomalous). When $n \geq 0.85$, it is case-II transport [13, 15]. Most HA and HA/PVA nanocomposites followed a non-Fickian release diffusion mechanism.

Conclusion

DSC, FTIR, and XRD results show that the main chemical components of the prepared materials are HA. In addition, the successful loading of the drug into nanocomposites was confirmed by the FTIR study. The in vitro dissolution indicated the prolonged sustained release of RIF over 8 h, which also followed the Higuchi ($r^2 = 0.8676, -0.9877$) and Korsmeyer–Peppas model ($r^2 = 0.9233–0.9635$) the diffusion component is between 0.43 and 0.85, which indicates non-fickian diffusion mechanism. Among the five different kinetic models, when respective correlation coefficients were compared to RIF release from HA, HA/PVA nanocomposites were found Higuchi and Korsmeyer-Peppas release model as the best. The most appropriate model was chosen according to the regression coefficients (r^2 values). k_0 values were specified by placing the release data in the respective equations and offered in Table 1, together with the regression coefficients (r^2). The data were analyzed for 100% drug release. The results of kinetic models showed that the release of RIF from HA/RIF, and HA/PVA/RIF samples followed the Higuchi model and HA/PVA/RIF loaded samples followed the Korsmeyer-Peppas model. Furthermore, the Higuchi model describes the release processes under the control of drug diffusion. From the kinetic study results, we concluded that RIF-loaded marine-based nanocomposite at pH 7.4 media showed low drug release characteristics. Therefore, this type of potential drug delivery system made of biodegradable and biocompatible polymers can be developed for sustained release of other drugs.

Supplementary Information The online version contains supplementary material available at https://doi.org/10.1007/s41779-022-00739-w.

Funding This work was supported by Marmara University Scientific Research Committee, Istanbul, Turkey, as SAG-D- 110618–0326 numbered projects.

Declarations

Conflict of interest The authors declare no competing interests.

References

1. Lertcumfu, N., Jaita, P., Manotham, S., Jarupoom, P., Eitssayeam, S., Pengpat, K., Rujijanagul, G.: Properties of calcium phosphates ceramic composites derived from natural materials. Ceram. Int.

42, 10638–10644 (2016). https://doi.org/10.1016/j.ceramint.2016.03.162
2. Udhayakumar, G., Muthukumarasamy, N., Velauthapillai, D., Santhosh, S.B.: Highly crystalline zinc incorporated hydroxyapatite nanorods' synthesis, characterization, thermal, biocompatibility, and antibacterial study. Appl. Phys. A Mater. Sci. Process. **123**(655), 1–9 (2017). https://doi.org/10.1007/s00339-017-1248-z
3. Jafari, S., Adipkia, K.: Application of hydroxyapatite nanoparticle in the drug delivery systems. J. Mol. Pharm. Org. Process Res. (2015) 1–2. https://doi.org/10.4172/2329-9053.1000e118.
4. Tămăşan, M., Ozyegin, L.S., Oktar, F.N., Simon, V.: Characterization of calcium phosphate powders originating from Phyllacanthus imperialis and Trochidae Infundibulum concavus marine shells. Mater. Sci. Eng. C. **33**(5), 2569–2577 (2013). https://doi.org/10.1016/j.msec.2013.02.019
5. Sadjadi, M.S., Meskinfam, M., Sadeghi, B., Jazdarreh, H., Zare, K.: In situ biomimetic synthesis, characterization and in vitro investigation of bone-like nanohydroxyapatite in starch matrix. Mater. Chem. Phys. **124**(1), 217–222 (2010). https://doi.org/10.1016/j.matchemphys.2010.06.022
6. Kel, D., Gökçe, H., Bilgiç, D., Ağaoğullari, D., Duman, I., Öveçoğlu, M.L., Kayali, E.S., Kiyici, I.A., Agathopoulos, S., Oktar, F.N.: Production of natural bioceramic from land snails. Key Eng. Mater. **493**(494), 287–292 (2012). https://doi.org/10.4028/www.scientific.net/KEM.493-494.287
7. Oktar, F.N., Gokce, H., Gunduz, O., Sahin, Y.M., Agaogullari, D., Turner, I.G., Ozyegin, L.S., Ben-Nissan, B.: Bioceramic production from giant purple barnacle (Megabalanus tintinnabulum). Key Eng. Mater. **631**, 137–142 (2015). https://doi.org/10.4028/www.scientific.net.KEM.631.137
8. Lopez, J.A., Munoz, J.A., Betancur, A.L., Ruiz, A.V., Orozco, J.M., Saldana, J.: Synthesis, characterization and ın vitro study of synthetic and bovine-derived hydroxyapatite ceramics: a comparison. Materials. **11**(333), 1–17 (2018). https://doi.org/10.3390/ma11020333
9. Cesur, S., Oktar, F.N., Ekren, N., Kilic, O., Alkaya, D.B., Seyhan, S.A., et al.: Preparation and characterization of electrospun polylactic acid/sodium alginate/orange oyster shell composite nanofiber for biomedical application. J Aust Ceram Soc. (2019). https://doi.org/10.1007/s41779-019-00363-1
10. Prasanna, A.P.S., Venkatasubbu, G.D.: Sustained release of amoxicillin from hydroxyapatite nanocomposite for bone infections. Prog. Biomater. **7**(4), 289–296 (2018). https://doi.org/10.1007/s40204-018-0103-4
11. Moreno-Vega, A.I., Gómez-Quintero, T., Nuñez-Anita, R.E., Acosta-Torres, L.S., Castaño, V.: Polymeric and ceramic nanoparticles in biomedical applications. J. Nanotechnol. **2012**, 1–10 (2012). https://doi.org/10.1155/2012/936041
12. Habraken, W.J.E.M., Wolke, J.G.C., Jansen, J.A.: Ceramic composites as matrices and scaffolds for drug delivery in tissue engineering. Adv. Drug Deliv. Rev. **59**(4–5), 234–248 (2007). https://doi.org/10.1016/j.addr.2007.03.011
13. Stipniece, L., Narkevica, I., Sokolova, M., Locs, J., Ozolins, J.: Novel scaffolds based on hydroxyapatite/poly(vinyl alcohol) nanocomposite coated porous TiO2ceramics for bone tissue engineering. Ceram. Int. **42**(1), 1530–1537 (2016). https://doi.org/10.1016/j.ceramint.2015.09.101
14. Cesur, S., Cam, M.E., Sayın, F.S., Su, S., Harker, A., Edirisinghe, M., Gunduz, O.: Metformin-loaded polymer-based microbubbles/nanoparticles generated for the treatment of type 2 diabetes mellitus. Langmuir (2021). https://doi.org/10.1021/acs.langmuir.1c00587
15. Baker, M.I., Walsh, S.P., Schwartz, Z., Boyan, B.D.: A review of polyvinyl alcohol and its uses in cartilage and orthopedic applications. J. Biomed. Mater. Res. - Part B Appl. Biomater. 100(5) (2012) 1451–1457. https://doi.org/10.1002/jbm.b.32694.
16. Cesur, S., Cam, M.E., Sayın, F.S., Su, S., Gunduz, O.: Controlled release of metformin loaded polyvinyl alcohol (PVA) microbubble/nanoparticles using microfluidic device for the treatment of type 2 diabetes mellitus. In Proceedings of the Lecture Notes in Computer Science (Including Subseries Lecture Notes in Artificial Intelligence and Lecture Notes in Bioinformatics); Springer: Cham, Switzerland, 2020; Volume 12108, pp. 185–193
17. Mollazadeh, S., Javadpour, J., Khavandi, A.: In situ synthesis and characterization of nano-size hydroxyapatite in poly(vinyl alcohol) matrix. Ceram. Int. **33**(8), 1579–1583 (2007). https://doi.org/10.1016/j.ceramint.2006.06.006
18. Lin, K., Chang, J.: Structure and properties of hydroxyapatite for biomedical applications. İn: Hydroxyapatite Biomed. Appl., Woodhead Publishing Series in Biomaterials, (2015). https://doi.org/10.1016/B978178242033000001-8.
19. Barzegar-Jalali, M., Adibkia, K., Valizadeh, H., Shadbad, M.R.S., Nokhodchi, A., Omidi, Y., Mohammadi, G., Nezhadi, S.H., Hasan, M.: Kinetic analysis of drug release from nanoparticles. J. Pharm. Pharm. Sci. **11**(1), 167–177 (2008)
20. Dash, S., Murthy, P.N., Nath, L., Chowdhury, P.: Kinetic modeling on drug release from controlled drug delivery systems. Acta Pol. Pharm. - Drug Res. **67**(3), 217–223 (2010)
21. O'Neil, M.J.: The Merck Index: an Encyclopedia of Chemicals, Drugs, and Biologicals. 13th Edition, Drug Dev. Res. (2006). https://doi.org/10.1002/ddr.20159.
22. Akyol, S., Ben-Nissan, B., Karacan, I., Yetmez, M., Gokce, H., Sugget, D.J., Oktar, F.N.: Morphology, characterization, and conversion of the corals Goniopora spp. and Porites cylindrica to hydroxyapatite. J Aust Ceram Soc. 55 (2019) 893–901.
23. Macha, I.J., Ozyegin, L.S., Chou, J., Samur, R., Oktar, F.N., Ben-Nissan, B.: An alternative synthesis method for di calcium phosphate (monetite) powders from mediterranean mussel (mytilus galloprovincialis) shells. J. Aust. Ceram. Soc. **49**(2), 122–128 (2013)
24. Karacan, I., Gunduz, O., Ozyegin, L.S., Gokce, H., Ben-Nissan, B., Akyol, S., Oktar, F.N.: The natural nano-bioceramic powder production from organ pipe red coral (Tubipora musica) by a simple chemical conversion method. J Aust Ceram Soc **54**, 317–329 (2018). https://doi.org/10.1007/s41779-017-0156-1
25. Williams, R.L., Hadley, M.J., Jiang, P.J., Rowson, N.A., Mendes, P.M., Rappoport, J.Z., Grover, L.M.: Thiol modification of silicon-substituted hydroxyapatite nanocrystals facilitates fluorescent labelling and visualisation of cellular internalisation. J. Mater. Chem. B. **1**, 4370–4378 (2013). https://doi.org/10.1039/c3tb20775g
26. Amarnath Praphakar, R., Sumathra, M., Sam Ebenezer, R., Vignesh, S., Shakila, H., Rajan, M.: Fabrication of bioactive rifampicin loaded κ-Car-MA-INH/Nano hydroxyapatite composite for tuberculosis osteomyelitis infected tissue regeneration. Int. J. Pharm. **565**, 543–556 (2019)
27. Hiremath, S.P., Saha, R.N.: Design and study of rifampicin oral controlled release formulations. Drug Delivery **11**(5), 311–317 (2004). https://doi.org/10.1080/10717540490494087
28. Doana, T.V.P., Coueta, W., Olivier, J.C.: Formulation and in vitro characterization of inhalable rifampicin-loaded PLGA microspheres for sustained lung delivery. Int J Pharm. **414**, 112–117 (2011). https://doi.org/10.1016/j.ijpharm.2011.05.007
29. Xue, K., Teng, S.H., N, N., Wang, P.: Biomimetic synthesis of novel polyvinyl alcohol/hydroxyapatite composite microspheres for biomedical applications. Mater. Res. Express. 5 (2018) 115401. https://doi.org/10.1088/2053-1591/aadc7d.
30. Aydın, N.E.: 5-FU drug loading during the production of hydroxyapatite-gelatin and hydroxyapatite-chitosan biocomposites in the simulated body fluid medium and drug release studies. Erzincan Univ. J Sci. Technol. **11**(3), 587–605 (2018). https://doi.org/10.18185/erzifbed.413332

31. Xu, Y., An, L., Chen, L., Cao, L., Zeng, D., Wang, G.: A Facile chemical route to synthesize Zn doped hydroxyapatite nanorods for protein drug delivery. Mater. Chem. Phys. **214**, 359–363 (2018). https://doi.org/10.1016/j.matchemphys.2018.04.117
32. Verma, A., Riaz, U.: Sonolytically intercalated poly(anisidine-co-toluidine)/bentonite nanocomposites: pH responsive drug release characteristics. J. Drug Deliv. Sci. Technol. **48**, 49–58 (2018). https://doi.org/10.1016/j.jddst.2018.08.024
33. Sheth, U., Nagane, R., Bahadur, P., Bahadur, A.: Salt effect on solubilization of hydrophobic drugs in block copolymeric micelles and investigation of their in vitro and in vivo oral efficiency. J. Drug Deliv. Sci. Technol. **39**, 531–541 (2017). https://doi.org/10.1016/j.jddst.2017.05.007
34. Golshan, M., Salami-Kalajahi, M., Mirshekarpour, M., Roghani-Mamaqani, H., Mohammadi, M.: Synthesis and characterization of poly(propylene imine)-dendrimer-grafted gold nanoparticles as nanocarriers of doxorubicin. Colloids Surfaces B Biointerfaces. **155**, 257–265 (2017). https://doi.org/10.1016/j.colsurfb.2017.04.029